Shock tube/time-of-flight mass spectrometer for high temperature kinetic studies

Robert S. Tranter[a] and Binod R. Giri
Chemistry Division, Argonne National Laboratory, 9700 South Cass Avenue, Argonne, Illinois 60439-4831

John H. Kiefer
Department of Chemical Engineering, University of Illinois at Chicago, 810 S. Clinton Street, Chicago, Illinois 60607

(Received 19 October 2006; accepted 4 January 2007; published online 9 March 2007)

A shock tube (ST) with online, time-of-flight mass spectrometric (TOF-MS) detection has been constructed for the study of elementary reactions at high temperature. The ST and TOF-MS are coupled by a differentially pumped molecular beam sampling interface, which ensures that the samples entering the TOF-MS are not contaminated by gases drawn from the cold end wall thermal boundary layer in the ST. Additionally, the interface allows a large range of postshock pressures to be used in the shock tube while maintaining high vacuum in the TOF-MS. The apparatus and the details of the sampling system are described along with an analysis in which cooling of the sampled gases and minimization of thermal boundary layer effects are discussed. The accuracy of kinetic measurements made with the apparatus has been tested by investigating the thermal unimolecular dissociation of cyclohexene to ethylene and 1,3-butadiene, a well characterized reaction for which considerable literature data that are in good agreement exist. The experiments were performed at nominal reflected shock wave pressures of 600 and 1300 Torr, and temperatures ranging from 1260 to 1430 K. The rate coefficients obtained are compared with the earlier shock tube studies and are found to be in very good agreement. As expected no significant difference is observed in the rate constant between pressures of 600 and 1300 Torr. © *2007 American Institute of Physics.*
[DOI: 10.1063/1.2437150]

I. INTRODUCTION

Shock tubes are versatile, well characterized tools that find extensive use in the study of gas phase reactions at high temperatures. The importance of shock tube techniques to the field of combustion and gas kinetics has been discussed in a number of reviews and texts (see, for example, Refs. 1–5) and their importance to combustion is further highlighted in compilations[6,7] of kinetic data for combustion where a large proportion of the information is drawn from shock tube studies. The primary advantage of the shock tube is that very high reaction temperatures over a large pressure range are attained effectively instantaneously in homogeneous, gaseous mixtures. Behind reflected shock waves these conditions normally persist for up to several milliseconds before they are quenched by rarefaction waves generated in the shock tube.[4] Nonetheless, the short observation times and high temperatures in a shock tube require fast, sensitive detection methods to accurately monitor the rapidly changing mixture composition from which kinetic and mechanistic information are elucidated.

A time-of-flight mass spectrometer (TOF-MS) can measure the concentrations of all species in a shock tube with sufficient time resolution for kinetic measurements. A number of groups[8–16] have constructed shock tubes with mass spectrometetric detectors, primarily evolutions of the instrument of Bradley and Kistiakowsky originally constructed in the early 1960s.[8] However, only Kern *et al.*[13] has pursued the technique extensively. The usefulness of the shock tube (ST)/TOF-MS in high temperature kinetics is nicely illustrated by the first observation of the formation of benzene from propargyl radicals by Kern *et al.*[17] This is currently considered a key step in soot production and has subsequently been extensively studied; see, for example, Refs. 18–22 and references therein.

As with any high-speed technique, there are a number of limitations and difficulties to be overcome with the shock tube/mass spectrometer combination. Amongst these are the sampling of gases from the shock tube, the vast operating pressure differential between the shock tube and MS, the rate at which spectra can be generated, the large quantity of data to acquire, and the inherent single shot nature of shock tubes.

A new ST/TOF-MS has now been constructed primarily for application to high temperature reactions of importance in combustion. The apparatus takes advantage of modern instrumentation to enhance the data acquisition rate of the mass detector, to improve the sampling of the gases from the shock tube, and to simplify the operation; see Ref. 9 for an enchanting description of the complexities of an early ST/TOF-MS. The shorter time intervals in the new instrument improve the resolution in the early stages of reaction from which rate coefficients can be best determined for the initial reactions. The sampling interface between the shock tube

[a]Author to whom correspondence should be addressed; electronic mail: tranter@anl.gov

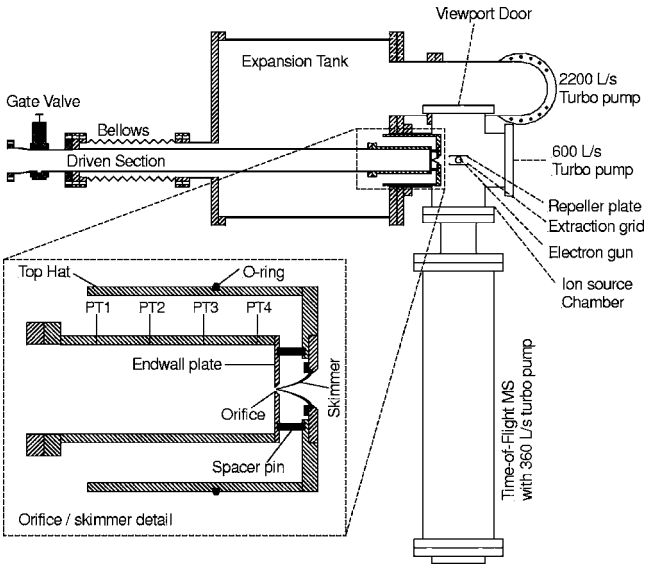

FIG. 1. Schematic of ST/TOF-MS assembly. A detail of the nozzle/skimmer arrangement is shown in the inset figure. PT1–PT4 are the PCB 132A35 pressure transducers for shock velocity measurement. For clarity, the end wall pressure transducer, PT5, is not shown. The electron gun is mounted on top of the ion source chamber pointing into the page; the location of the electron gun is marked by the dashed circle.

and TOF-MS has been designed to minimize the effects of the end wall thermal boundary layer that can severely compromise chemical kinetic measurements. Furthermore, this interface increases the range of pressures, compared, say, to the apparatus of Kern *et al.*[13] that can be generated in the shock tube to over 10^3 Torr, yet remains compatible with the necessary high vacuum in the TOF-MS, $<10^{-5}$ Torr. The new ST/TOF-MS is described along with results of experiments on the pyrolysis of cyclohexene which provides a rigorous test of the apparatus.

II. EQUIPMENT DESIGN

The ST/TOF-MS apparatus is most easily described by considering it as several separate parts: the shock tube, the TOF-MS, the interface connecting them, and the data acquisition system. A schematic of the interface and the arrangement of the shock tube and TOF-MS is shown in Fig. 1. In addition to the equipment, the molecular beam sampling via the interface and end wall boundary layer effects in the shock tube are discussed below.

A. Shock tube

The theory, design, and operation of shock tubes have been extensively described; see, for example, Ref. 4 and references therein. The current shock tube has been designed for two experiments, both mass spectrometry behind reflected shock waves and laser schlieren (LS) behind incident shock waves. These experiments can be performed over a wide range of temperature limited only by the time resolution of the technique. However, LS experiments are normally limited to pressures <1 atm due to turbulent boundary layer development behind the incident shock wave deflecting the laser beam, whereas the TOF-MS experiments can easily be extended to pressures of several atmospheres, primarily limited by the available pumping capacity. Currently, the TOF-MS and LS experiments are run separately but a reconfiguring of the TOF-MS interface to permit simultaneous LS and TOF-MS experiments behind incident shock waves is anticipated in the near future.

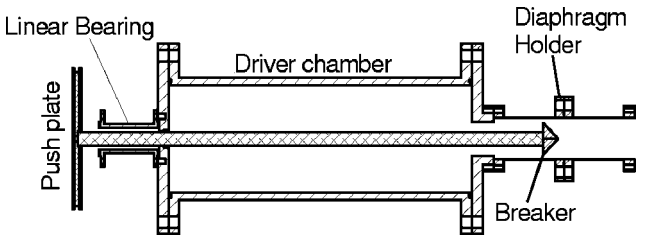

FIG. 2. Schematic of the driver section. Force is applied to the "push plate" to break the diaphragm and fire the shock tube.

The shock tube consists of two stainless steel tubes, the driver and driven sections, separated by an aluminum diaphragm. The driver section, Fig. 2, is a little unusual in that it is short and wide, 78×20 cm inside diameter (i.d.). A short section of 7.1 cm i.d. tube connects the driver section to the driven section and terminates in the flanges that hold the diaphragm. A shaft, externally supported by a linear bearing, is inserted through the back wall of the driven section, Fig. 2. A four bladed, sharp tipped diaphragm breaker is attached to the front of the shaft and slices open the aluminum diaphragms. No fragments break away from the diaphragms when they open, which is important as fragments could block or damage the sampling orifice to the TOF-MS. The driver section is equipped with a number of ports that are used for admitting helium, venting, monitoring pressure (Sensotec SC-500), and evacuating via an oil pump (Welch 1376 with foreline trap). The pump is isolated from the driver section by a solenoid actuated ball valve that can be remotely operated.

The squat driver section has been chosen for two reasons. Firstly, in the TOF-MS and LS experiments rapid quenching of the reaction zones by rarefaction waves is not required, cf. single pulse shock tubes, because the experiments are terminated before the rarefaction waves arrive. Thus it is sufficient to ensure that there is enough driver gas available to sustain the shock wave without significant attenuation, and that the driven section is sufficiently long for a well-developed shock wave to form and give the desired observation time. These criteria can be achieved with a short, wide driver that occupies little space. Secondly, the driver section will ultimately be converted to make a diaphragmless shock tube using a modified version of that of Hurst and Bauer.[23] The existing driver and shaft are key parts of the diaphragmless system that will be implemented now that the TOF-MS and sampling interface are completed. The main advantages of a diaphragmless shock tube are that the possibility of fragments is eliminated, shock conditions are more reproducible between experiments, and the interior of the shock tube is not exposed to the laboratory atmosphere between experiments.

The driven section consists of two parts. The first is 595 cm long, 7.1 cm i.d., and has a pair of optical ports (quartz, 27 mm wide, 7 mm thick) centered 498 cm from the

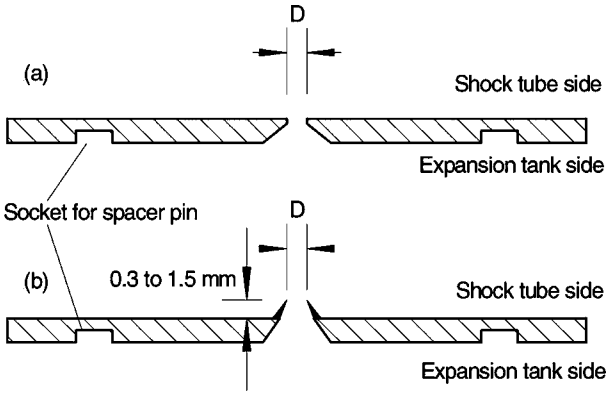

FIG. 3. Two styles of driven section end plates. (a) Type *A*: flat plate with divergent nozzle counter bored into the plate. (b) Type *B*: the diverging nozzle protrudes into the shock tube effectively moving the sample point away from the end wall. Type *B* plates are normally made with replaceable nozzles. Both types of end plates were used in this work; see text for details.

diaphragm. A set of six pressure transducers (Dynasens CA-1135), spaced 120 mm between transducer centers, is located around the optical ports. These pressure transducers and windows are primarily for use with LS experiments. The last 20 cm of this section consists of a T piece which provides a connection to the mixing rig and pumps. From our experience with LS experiments we have found it beneficial to locate the mixing rig and pumping ports downstream of the LS observation point to minimize disturbances in the incident shock wave that are detectable with the extremely sensitive LS technique. The TOF-MS experiments have proven to be insensitive to these disturbances, presumably because samples are withdrawn from the center of the shock tube and sidewall artifacts, to which LS is sensitive, have little effect. Thus the mixing rig/pump connection has been placed between the LS and TOF-MS observation points. At the end of the first part of the driven section a conical reducer makes a smooth transition from 7.1 to 6.1 cm i.d. tube and the shock tube extends by another 120 cm into the TOF-MS interface. The reduction in tube diameter is imposed by the i.d. of the feedthrough bellows into the TOF-MS interface, see Fig. 1. A gate valve is located immediately after the reducer and can be used to isolate the TOF-MS interface from the rest of the shock tube. The driven section is terminated by a stainless steel end plate with an orifice centered in the plate that forms the entrance to the shock tube/TOF-MS interface. Two styles of end plate, types *A* and *B*, see Fig. 3, were used in the development of the ST/TOF-MS. The flat plate, type *A* Fig. 3, is now used for most experiments although a number of type *B* plates with different cone geometries have been tried.

The postshock conditions (temperature, pressure, and density) are obtained in the normal way from the ideal shock wave expressions[4] using the initial temperature, T_1, and pressure, P_1, in the driven section, the measured incident shock wave velocity, and the heat capacities of the gases. The velocity is calculated from the time taken for the shock wave to travel between successive pressure transducers and is measured with timers that are accurate to 0.1 μs. In LS experiments the pressure transducers upstream of the reducer are used to trip the timers. However, in the TOF-MS experiments, the sampling point is far from the LS transducers and the shock wave might accelerate as it passes through the reducer. To obtain accurate velocities close to the sampling point in the TOF-MS experiments another set of miniature pressure transducers (PCB 132A35, identified as PT1–PT4 in Fig. 1) was installed in the sidewall of the driven section inside the expansion tank of the interface. These transducers are spaced 76.2 mm between centers and PT4 is positioned approximately 27 mm from the end plate. A fifth pressure transducer, PT5, is installed in the end plate coaxial with the shock tube. Thus the incident and reflected shock velocities can also be obtained close to the end wall of the driven section and then used to calculate the temperature, T_5, and pressure, P_5, behind the reflected shock wave. Comparing the velocities measured with the LS (upstream) pressure transducers and the TOF-MS pressure transducers shows an increase in shock velocity of around 10% in the narrower part of the driven section. Little attenuation is evident in the velocity measurements made by either set of transducers.

The shock velocity measurement and subsequent calculation of T_5 and P_5 is one of the most critical aspects of the experiment. Thus the timer circuits are periodically checked by simultaneously capturing the output of a selected pair of pressure transducers with a digitizer (Compuscope 14100, GAGE Appplied Inc.) and calculating the time interval from the recorded signals.

The driven section is filled and evacuated via the mixing rig which can be isolated from the shock tube with a high vacuum valve. The pumping system consists of an oil pump (Leybold D16B with foreline trap) and a turbopump (Leybold Turbovac 150). These are sufficient to evacuate the driven section and mixing rig to around 10^{-5} Torr. Pressures in the mixing rig and loading pressures in the driven section are monitored by two capacitance manometers (Leybold Ceravac 90).

When the driven section is filled and the gate valve is open, gas continually leaks through the orifice and any consequent drop in P_1 needs to be considered. In fact, the orifice in the nozzle plate is sufficiently small that the change in pressure inside the shock tube between filling and firing the shock tube is <0.1 Torr. This small pressure drop corresponds to $<0.5\%$ change in the calculated P_5 and introduces no error in the calculation of T_5, as this depends on the incident shock Mach number and T_1, not P_1.[4] Thus only P_5 is affected and this change is negligible. The gas eluting from the orifice will also induce a small flow in the bulk gas in the driven section which might cause a small change in the shock velocity and hence T_5 and P_5 near the end plate. The resulting perturbation of conditions behind the reflected shock wave can be obtained by estimating the velocity induced in the reflected shock region by the mass flow through the orifice. The induced velocity, u_i, can be calculated by using the following equation:[24]

$$u_i = \left(\frac{2}{\gamma+1}\right)^{(\gamma+1)/2(\gamma-1)} \left(\frac{D}{D_{\text{plate}}}\right)^2 \sqrt{\frac{\gamma R T_5}{W}}, \tag{1}$$

where W is the molar average molecular weight, R the universal gas constant, D and D_{plate} are, respectively, the orifice and the end plate diameters, and γ the specific heat ratio of

the mixture. For the operating conditions of the ST/TOF-MS, u_i is negligible.

B. Interface

A schematic of the differentially pumped interface between the TOF-MS ion source chamber and shock tube is shown in Fig. 1, with a detail of the nozzle/skimmer arrangement shown in the inset. The ion source chamber is a six way cross of which one arm is bolted to a port on the exit of the 110 L expansion tank that forms the first stage of the interface and a turbopump (Leybold Turbovac 600 backed by a D16B forepump with foreline trap) is mounted opposite. On the top of the cross is an electron gun and an ion gauge is located on the bottom arm. One arm in the orthogonal plane to the shock tube is connected to the TOF-MS and the final arm is closed by a viewport door that gives optical and physical access to the ion source chamber.

The connection between the expansion tank and the ion source chamber is made from a replaceable, conical nozzle referred to as the skimmer (Beam Dynamics Inc. model 2), inset Fig. 1. This skimmer is clamped in a shallow counterbore above a hole centered on a plate closing one end of a short piece of stainless steel tube, labeled "Top Hat" in Fig. 1. This tube slides on an O ring in the arm of the ion source attached to the expansion tank, allowing the position of the skimmer exit in the ion source chamber to be adjusted.

The driven section of the shock tube enters the expansion tank, opposite the skimmer, via an edge welded bellows and passes through the tank into the Top Hat to which it is attached by a clamp (not shown). The orifice in the end of the driven section is aligned with the skimmer, and the alignment and separation between the nozzle and skimmer are set and maintained by spacer pins, Fig. 1. The separation, determined by extensive experimentation with different spacings and reaction conditions, is currently set at $\approx$3 mm.

The nozzle/skimmer unit has been constructed so that it can be assembled outside of the ST/TOF-MS and inserted as a single piece into the arm of the ion source chamber through the expansion tank, Fig. 1. The assembly is then joined to the end of the driven section that extends through the bellows. This facilitates changing the nozzle and skimmer, cleaning the end of the driven section of the shock tube, and checking the nozzle/skimmer alignment. Additionally, the PCB pressure transducers are mounted on this section and thus can easily be replaced as needed. The transducers are connected to the power supplies and timers by a multipin, vacuum-instrument feedthrough mounted on the expansion tank.

The ion source chamber is evacuated by the turbopump mounted on the cross opposite the connection to the expansion tank. A large turbopump (Pfeiffer Balzers TPU 2200 backed by an oil pump with foreline trap) evacuates the expansion tank. This pump is connected to the expansion tank via an 8 in. Conflat port and elbow which does somewhat restrict the conductance to the pump. However, even at the highest loading pressures in the current work, $P_1=30$ Torr, the pumping arrangement is sufficient to keep the pressure $<10^{-4}$ Torr in the expansion tank prior to firing. A future modification may include coupling the large turbopump directly to the expansion tank with a larger diameter port which would further improve the effective pumping speed.

The TOF-MS, interface, and pumps are all mounted on a custom frame with three-axis adjustment and the bellows at the entrance to the expansion tank allows small misalignments between the expansion tank and shock tube to be accommodated. Furthermore, the separation between the skimmer and ion source can be adjusted while the equipment is under vacuum and observed through the viewport door, Fig. 1.

A number of previous ST/TOF-MS systems[9–13] used an end plate similar to type *B*, Fig. 3. The small truncated cone protruded into the shock tube in an attempt to increase the observation time before the end wall thermal boundary layer dominated the sampled gases. However, Krizancic *et al.*[14] constructed a ST/TOF-MS with differential pumping, which permits nozzles with larger diameter orifices to be used, and found no difference between experimental results obtained with end plates similar to both types *A* and *B* in Fig. 3. In this work we have tested many styles of cone on a type *B* end plate and agree with the conclusions of Krizancic *et al.*[14] Type *A* plates are preferable in a differentially pumped ST/TOF-MS due to their ease of manufacture and durability. We also found that a too large type *B* cone lowered the measured rate coefficients considerably, presumably due to poor reflection of the shock wave in the region of the cone. The orifice in the present nozzle plate has an area at least 16 times greater than that in the earlier instruments, although the maximum mass flux though the nozzle is restricted somewhat by the aspect ratio (orifice diameter/orifice wall thickness) of 0.8.

The final part of the interface is the skimmer. In this work skimmers with three different entrance diameters, 0.32, 0.48, 0.79 mm, have been used. Under most circumstances the 0.79 mm skimmer was too large with excessive gas flow into the TOF-MS; for $P_5<200$ Torr it may still prove useful. Both of the smaller skimmers have proved satisfactory for $P_5>200$ Torr.

C. TOF-MS

The general theory and operating principles of time-of-flight mass spectrometers are well described in the literature; see, for example, Ref. 25 and references therein. The present TOF-MS is a R. M. Jordan reflectron mass spectrometer equipped with an 18 mm Chevron-stack multichannel plate (MCP) detector for use in linear mode, and a 40 mm Chevron-stack MCP for reflectron mode. The flight tube has been shortened to 38.1 cm to reduce analysis times. The elementary reactions that we anticipate studying in the ST/TOF-MS generally involve species whose ions have m/z less than $\approx$200, so the decrease in mass resolution with the shorter flight tube is not of concern as base line separation is maintained for differences in m/z of 1 amu. For studies involving heavier species the original flight tube, 82 cm long, can easily be reinstalled. The only other change to the TOF-MS is that a second set of steering plates mounted closer to the flight tube than the original steering plates has been installed. Due to the internal construction of the TOF-MS the original steering plates caused the ion beam to

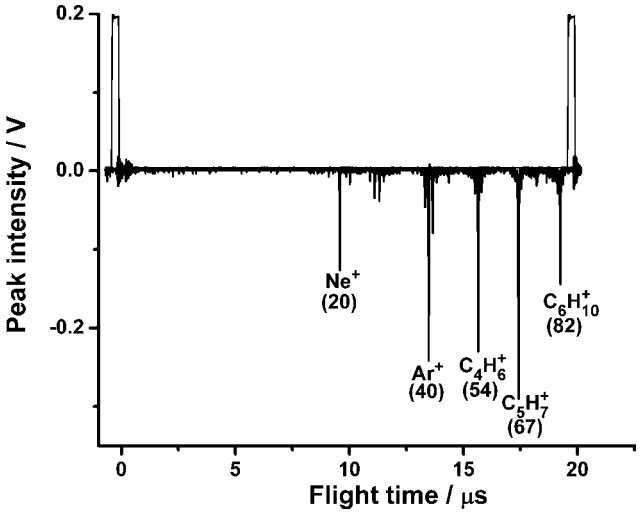

FIG. 4. A 20 μs time segment acquired at an ionization cycle of 50 kHz showing the fragments of cyclohexene. Neon was the bath gas and argon was added to the mixture as an internal standard. Here T_5=1129 K, too low for reaction, and P_5=684 Torr. The numbers in the parentheses represent m/z values for the indicated ions. The flight times are measured from the injection pulse, the falling edge of the square pulse at t=0.

collide with a wall at the larger angles needed to focus the ions onto the MCP in the shortened TOF-MS. The location of the new steering plates solves this problem.

The nozzle/skimmer interface between the shock tube and TOF-MS forms the gases eluting from the shock tube into a molecular beam. Concentrations of species in the molecular beam and, hence, in the shock tube are determined by electron impact (EI) ionization of a fraction of the molecular beam followed by mass analysis. Ions are generated in the ion source which consists of a repeller plate, extraction grid, and an electron gun, E-gun, mounted orthogonal to the flight tube of the TOF-MS on the top of the ion source chamber, see Fig. 1. At the exit of the electron gun there is a split plate, one-half of which is connected to the repeller and the other to the extractor. The electron beam from the E-gun passes through a gap between the halves of the split plate into the ion source. The TOF-MS is perpendicular to both the shock tube and the E-gun and the ion source is aligned so that the molecular beam flows between the repeller plate and extraction grid. The molecules that are not ionized are evacuated by the turbopump opposite the skimmer, see again Fig. 1.

The well defined ion packets required for analysis are formed by pulsing the electron beam in and out of the space between the repeller plate and extraction grid. This is achieved by periodically changing the voltage applied to the extraction grid. Initially, the repeller plate and extraction grid are at the same voltage, typically $\approx$1800 V, and the two halves of the split plate on the E-gun are balanced allowing electrons into the ionization zone where they interact with the molecular beam. After a short period, typically 0.4 μs, the voltage at the extraction grid is dropped by 300–400 V and the split plate becomes unbalanced. This deflects the electron beam out of the ionization volume and onto the split plate. The potential gradient between the repeller and extractor draws the positive ions through the extraction grid where

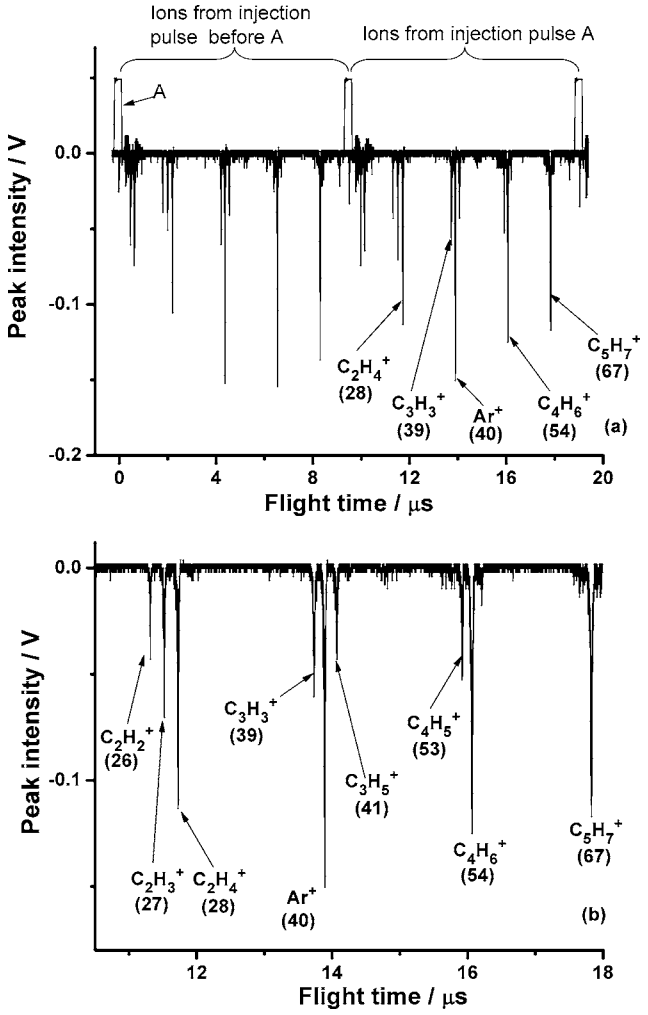

FIG. 5. (a) A 20 μs time segment where P_5=558 Torr, T_5=1360 K, and the ionization cycle was 105 kHz. The mass spectrum shows the fragments of cyclohexene and the reaction products. The numbers in parentheses represent the m/z value for the corresponding species. Flight times for the indicated species are relative to the injection pulse which is labeled A. The unlabeled peaks appearing at times less than 10 μs correspond to ions generated in the prior ionization event. (b) An expanded portion of (a) showing the base line separation between peaks differing by 1 amu.

they are accelerated to their final velocities and focused onto the detector with the remaining ion optics.

Adjusting the time interval between successive injection events alters the frequency that the molecular beam is probed and hence the time resolution in the concentration/time profiles of the gases in the shock tube. Short time intervals are desirable to obtain the most accurate picture of the rapidly changing concentrations inside the shock tube. With the current apparatus a maximum cycle frequency in the ion source of 195 kHz (5.12 μs) is achievable. However, at this rate ions from several ionization events become intermingled in the drift section of the TOF-MS resulting in multiple overlapping spectra and frequently saturation of the MCP. Typically the best operation is actually found when the ion source is pulsed at 105 kHz (9.52 μs). This still causes overlap of two successive spectra with light ions from one ionization event overtaking heavier ions from a prior event. Conditions are additionally selected to ensure that ions from different events do not arrive simultaneously at the detector. These

overlapping spectra can be easily separated using in-house software and a spectrum obtained corresponding to a low repetition rate where overlap does not occur. Spectra obtained at 50 and 105 kHz are shown in Figs. 4 and 5 and the ions from different events in the 105 kHz spectra are identified. Clearly ions from different ionization events do not interfere with each other.

Ionization energies in the range of 28–34 eV have been used in these experiments and work well for a wide variety of species. At 28 eV ionization of the bath gas neon is almost completely suppressed but signals for species of interest may be weak, whereas at 34 eV the neon peak may be excessively strong. As usual the exact operating conditions are a compromise between conflicting needs and have to be selected for the system of interest.

The TOF-MS flight tube is turbopumped (Leybold TurboVac 361 backed by a D16B oil pump with foreline trap). The configuration of the ion optics and low pressures in the ion source chamber and flight tube provide effective differential pumping between the chamber and flight tube. The background pressures in the ion source chamber and the flight tube are typically around $(1-3)\times10^{-8}$ Torr. During an experiment the pressure in the ion source will rise after a few tens of milliseconds (long after data acquisition has terminated) to over 10^{-4} Torr which is sufficiently high to cause arcing in the ion source. To prevent damage to the power supplies for the electron gun and ion source the electrical supply to the TOF-MS is cut shortly (<1 s) after firing a shock. Simultaneously, the solenoid valve on the driver section pump opens rapidly venting the shock tube minimizing pressure buildup in the TOF-MS.

D. Data acquisition

The passage of the incident shock wave over the first pressure transducer, PT1 (Fig. 1), not only starts the timing circuits that are used to obtain shock velocities but also generates a voltage pulse that is used to initiate both the ion generation/analysis cycles in the TOF-MS and the data acquisition. Following this trigger signal the TOF-MS pulse rate is controlled with a signal generator. PT1 is used to trigger data acquisition instead of the end wall pressure transducer, PT5, to ensure that a reasonable amount of both preshock and postshock data are captured. Up to 2 ms of data is acquired continuously after the trigger has occurred.

An Acqiris DP210 8 bit analog/digital (A/D) board acquires the MCP output at either 1 or 2 GS/s and an Acqiris DP306 12 bit A/D board captures the timing signal at 100 MS/s. The ions of discrete m/z strike the MCP in tight packets and generate peaks that are between 10 and 20 ns wide at full width half maximum, thus the DP210 board captures an adequate number of points to accurately reproduce the fine details in the peak shapes. The two boards are synchronized and use of a single trigger simplifies the alignment of the digitized signals from the DP210 and DP306 boards. An example of the raw data is shown in Fig. 6 and interpretation of these data is discussed later.

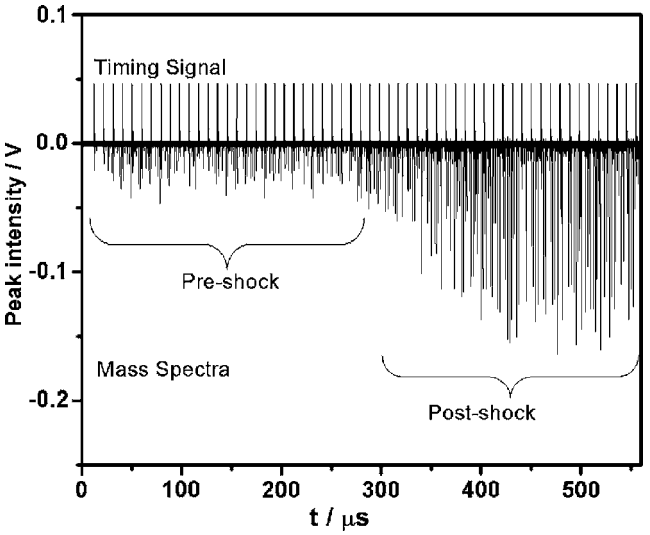

FIG. 6. Raw data obtained at an ionization cycle frequency of 105 kHz from a ST/TOF-MS experiment, $P_5=558$ Torr, $T_5=1360$ K. The downward spikes, labeled as mass spectra, show the preshock as well as the postshock data recorded on the DP210 board. The upward spikes show the timing signals recorded on the DP306 board. A single time segment from the postshock region of this experiment is shown in Fig. 5.

III. MOLECULAR BEAM SAMPLING FROM THE SHOCK TUBE

In the ST/TOF-MS experiments the zone behind the reflected shock wave acts as a high temperature, high pressure reservoir of gases. The diverging nozzle in the end plate of the driven section and the pressures in the shock tube and expansion tank, Fig. 1, are such that a supersonic jet is formed downstream of the nozzle. The literature on such gas jets and molecular beam sampling (MBS) is extensive; see, for example, Refs. 26–33 and the references therein. The particular case of sampling gases from a high pressure source into a mass spectrometer is treated in detail by Stearns *et al.*[30] Only the features of MBS most critical to successful operation of the ST/TOF-MS will be considered here.

For the ST/TOF-MS to be at all useful it is vital that the gas sample entering the ion source of the mass spectrometer accurately represents the gases withdrawn from the zone behind the reflected shock wave. There are two ways that a nonrepresentative sample might be obtained. Firstly, if the gases eluting from the tube are not rapidly quenched then reaction will continue in the molecular beam as the molecules travel to the ion source. Secondly, a thermal boundary layer (TBL) develops at the end plate after reflection of the incident shock wave. The temperature within the TBL can be much lower than T_5, and if gases are withdrawn from the TBL simultaneously with gases from behind the reflected shock wave then the apparent rate coefficients will be lower than obtained from samples drawn solely from behind the reflected shock wave.

A. Jet cooling

The large pressure ratio across the orifice, $>10^5$ for typical operating conditions, is sufficient to ensure a supersonic jet forms as gas flows and expands through the nozzle.

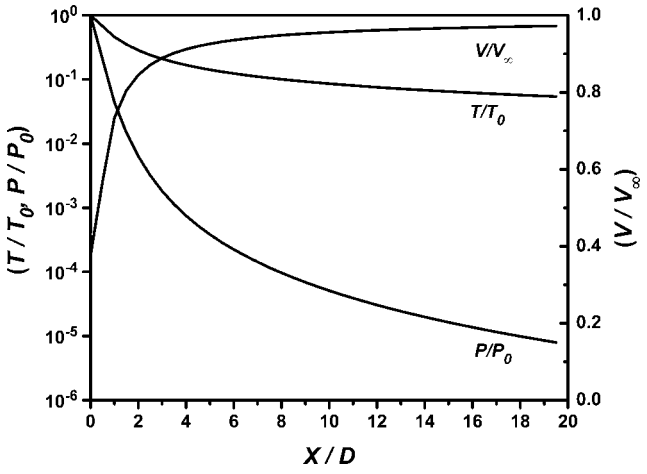

FIG. 7. Free jet centerline properties at various x/D, x the downstream distance from the nozzle orifice and D the nozzle diameter: Temperature, T, and pressure, P, along the jet line are normalized by the reservoir temperature, $T_0=T_5$, and pressure, $P_0=P_5$, and the centerline velocity by its maximum value, V_∞.

Various centerline properties of the jet were calculated for a range of x/D (x=distance from orifice and D=orifice diameter). The temperature, T, and pressure, P, relative to the source pressure, P_0, and temperature, T_0, were calculated from Eqs. (2) and (3).[29–31] Additionally, the gas jet velocity, V, relative to the terminal velocity, V_∞, was obtained from Eqs. (4) and (5).[29–31] The temperature and pressure of the reservoir were, respectively, set to typical conditions behind the reflected shock wave, $P_5=P_0=600$ Torr and $T_5=T_0=1500$ K; the subscript $_0$ denotes reservoir conditions chosen for consistency with the literature.

$$\frac{T}{T_0}=\left(1+\frac{\gamma-1}{2}M^2\right)^{-1}, \tag{2}$$

$$\frac{P}{P_0}=\left(\frac{T}{T_0}\right)^{\gamma/(\gamma-1)}, \tag{3}$$

$$V=M\left(\sqrt{\frac{\gamma RT_0}{W}}\right)\left[1+\frac{(\gamma-1)M^2}{2}\right]^{-0.5}, \tag{4}$$

$$V_\infty=\left[\frac{2R}{W}\left(\frac{\gamma}{\gamma-1}\right)T_0\right]^{0.5}. \tag{5}$$

M, the jet Mach number along the centerline,[29–31] was calculated using

$$M=\left(\frac{x}{D}\right)^{(\gamma-1)/j}\left[C_1+\frac{C_2}{x/D}+\frac{C_3}{(x/D)^2}+\frac{C_4}{(x/D)^3}\right]. \tag{6}$$

Here coefficients C_1-C_4 are tabulated in Table 2.2 of Ref. 31, $j=1$ for an axisymmetric nozzle,[31] and γ is the specific heat ratio of the mixture. The latter was set to 9/7 which is representative of the reacting mixtures used in this work.

The results of the calculations of P/P_0, T/T_0, and V/V_∞ are shown in Fig. 7. As can be seen in the figure at $x/D\approx 5$, the jet is close to terminal velocity and P and T have dropped rapidly and sufficiently to freeze the gas composition. Thus the concentrations in the molecular beam will accurately reflect those in the shock heated gases.

B. Thermal boundary layer effects

The growth of the TBL and its effect on ST/TOF-MS experiments has frequently been a topic of discussion.[8–14,34,35] A treatment was given by Dove and Moulton[9] who assumed that the samples were withdrawn from a hemisphere, radius r, centered on the orifice and that the TBL grew in thickness, δ, from the end wall into the shock heated gases. Thus the fraction of gases drawn from the TBL would increase in time. At some point $\delta>r$, all the samples will be drawn from the TBL. To extend the time before $\delta>r$ and thereby minimize TBL effects Dove and Moulton proposed using a small conical nozzle on the end plate, similar to type B of Fig. 3, which can crudely be considered to reduce δ by the height of the cone. Voldner and Trass[34,35] extended the ideas of Dove and Moulton to consider, amongst other things, more realistic streamlines, the effect of orifice size on the time at which δ becomes larger than r, and the structure of the supersonic jet. Furthermore, they examined the effect on the sample reaching the mass spectrometer of placing a skimmer in the supersonic jet. With regard to the present work, one of the most important conclusions of Voldner and Trass is that the time taken for the TBL to grow sufficiently thick to engulf the sampling zone is proportional to D to the fourth power,[34] where D is the orifice diameter. Thus larger orifices are preferred to minimize TBL effects. Additionally, Voldner and Trass showed that gases from the TBL are confined to the outer edges of the supersonic jet formed downstream of the orifice and that these can be prevented from entering the TOF-MS with a skimmer. In the current apparatus $D=0.4$ mm, considerably greater than in the nozzles used by Dove and Moulton[9] and Kern *et al.*,[13] where $D<0.1$ mm. Based on the formulas in Ref. 34, it is estimated that at least 30 ms would be required for the TBL to dominate the sampled gases from the new ST/TOF-MS. Whereas typically, the gases from behind the reflected shock wave are sampled for <1 ms. Furthermore, at the orifice the Knudsen number, Kn, is <0.003 (ratio of mean free path λ to D) at the above reservoir conditions. For $\mathrm{Kn}<0.02$ the flow through the nozzle is continuum and boundary layer effects due to the flow through the nozzle are insignificant.[26] Thus it can be concluded that the large orifice minimizes the contamination of the sampled gases with TBL gases and that a type A end plate will perform satisfactorily.

While a large orifice is useful to minimize TBL effects, the flow through the nozzle has implications for other aspects of the experiment that have to be considered when selecting the nozzle. The effect of the nozzle flow on P_1 and the incident shock velocity were discussed earlier and for the $D=0.4$ mm orifice was found to be negligible. Additionally, a large nozzle such as that used here requires either differential pumping between the shock tube and TOF-MS or a huge pumping capacity to maintain good vacuum in the TOF-MS. In this apparatus we have chosen to use differential pumping with a skimmer immersed in the supersonic jet. The effect of the skimmer on the gas sample will now be considered.

The skimmer of Fig. 1 takes a sample from the centerline of the supersonic jet, cutting off the outer part of the jet. The skimmer tip should be located between the orifice and Mach disk that bounds the downstream side of the jet in the

high density molecular flow region[30,31], often referred to as the "zone of silence." For typical conditions in the ST/TOF-MS the Mach disk forms at $x/D \approx 400$, using Eq. (7),[30,31] a considerably greater distance from the orifice than either the position of the skimmer tip, $x/D=8$, or the center of the ion source.

$$\text{Here } x/D = 0.67(P_0/P_b)^{0.5}, \tag{7}$$

where P_b=pressure in the expansion tank, typically $<10^{-4}$ Torr.

Furthermore, within the zone of silence optimum beam intensity and minimum skimmer-jet interaction are obtained when Kn_s, the Knudsen number at the skimmer entrance, is unity or slightly greater.[32,33] Kn_s has been calculated for pure neon and a mixture of 4% cyclohexene in neon, used as a test case in this work, for the centerline supersonic jet properties at the skimmer tip, $x/D=8$. For the skimmers used in this work Kn_s is close to unity.

To ensure that the outer parts of the supersonic jet are not sampled it is important that the gases passing through the skimmer come from close to the jet centerline. The fraction of the jet from the nozzle that passes through the skimmer into the ion source is given by[34]

$$f = \frac{m_s}{m} = \frac{M_s}{\alpha}\left(\frac{D_s}{D}\right)^2 \left\{ \frac{\gamma+1}{2}\left[1 + \frac{(\gamma-1)M_s^2}{2}\right]\right\}^{-(\gamma+1)/2(\gamma-1)}, \tag{8}$$

where m_s is the mass flow rate through the skimmer, m the mass flow rate through the nozzle, D_s the diameter of the skimmer opening, and M_s the local Mach number in the jet at the skimmer location obtained from Eq. (6). Here α =Liepmann's correction factor[36] which does not change significantly for different γ and the value for argon of 0.81 has been used.

For the skimmer location and jet described above, the result from Eq. (8) is that less than 1% of the nozzle flow passes through the skimmer into the mass spectrometer which corresponds to sampling within a few degrees of the jet centerline.[34,35] Thus with the nozzle and skimmer centers aligned the jet is sampled close to the flow centerline and the gases entering the ion source are not contaminated by TBL gases. Of course, the results of these above calculations are estimates of the jet behavior and are best confirmed by experiment. In the ST/TOF-MS this can be done most directly and unambiguously by measuring rate coefficients for a well characterized reaction.

IV. THERMAL DISSOCIATION OF CYCLOHEXENE

To test the performance of the ST/TOF-MS the dissociation of cyclohexene, reaction (9), has been studied. The reaction is well known to be a reverse Diels-Alder molecular elimination that forms two stable products, ethylene and 1,3-butadiene, in the temperature regime of interest. This reaction has been studied by several groups over a wide range of conditions and the data are in good agreement.[37–41]

$$C_6H_{10} \rightarrow C_4H_6 + C_2H_4 (\Delta H^o_{T,0\ \mathrm{K}} = 38\ \text{kcal/mol}). \tag{9}$$

While the reaction is simple, it actually forms a rather challenging experiment for the ST/TOF-MS, testing the capabilities of the instrument quite rigorously. The challenges arise due to the large activation energy, 65.7 kcal mol^{-1} and endothermicity of the reaction as well as application of the mass spectrometry as discussed below.

The high pressure limit rate coefficient for reaction (9), k_∞, from Kiefer and Shah[37] is given by the following expression:

$$\log[k_\infty(\text{s}^{-1})] = 15.57 - 65.7/(2.303RT); \tag{10}$$

here units are kcal, mol, and K. The large activation energy implies that the measured rate coefficients will be very sensitive to temperature. Consequently, if the TBL, where $T \ll T_5$, contaminates the gases entering the TOF-MS, the apparent rates of reaction should appear much lower than the literature values.

The concentration time profiles from which the rate coefficients are derived are obtained from the mass spectra for each ionization cycle. For the experiments reported here these mass spectra are complicated by extensive fragmentation of the molecules in the ion source which limits the identification of unique mass spectral features for tracking species. A time-of-flight mass spectrum for the reagent mixture used in this work with the major peaks identified is shown in Fig. 4; T_5 and P_5 were insufficient for reaction. It is clear that cyclohexene, $m/z=82$, fragments extensively with the major fragment appearing at $m/z=67$ and additional ions are seen at $m/z=54$, 39, and 27 in decreasing order of abundance, which agrees well with the literature electron impact mass spectrum.[42] The fragment $m/z=54$ corresponds to 1,3-butadiene which is also one of the reaction products. The literature mass spectrum for 1,3-butadiene[42] shows the largest peak at $m/z=39$ with a strong peak at $m/z=54$ (parent) and reasonably strong peaks at $m/z=28$ and 27. The largest peak in the mass spectrum of ethene, the second product of reaction (9), occurs at $m/z=28$ (parent), with strong secondary peaks at $m/z=27$ and 26.[42] Thus, of the major peaks, the only ones unique to any one species are those at $m/z=82$ and $m/z=67$. Both of these peaks are associated with cyclohexene and can thus be used to track its concentration. Although $m/z=67$ is the dominant peak from cyclohexene it only accounts for about 1/3 of the ions from C_6H_{10} and thus even this peak in the mass spectrum may be weak. As the reaction proceeds and cyclohexene is consumed the contribution of its fragments to the peaks representing other species will decrease. In principle a correction can be made to the various peak areas to account for the contributions from fragments arising from different parent species in the ion source. However, in these single shot shock tube experiments the statistical variations in spectra from different time periods (ionization/analysis cycles) are sufficiently large to render this approach unwise. Hence, in these experiments, rate coefficients have only been determined from the loss of cyclohexene and not the formation of the products; normally a valuable cross-check on the calculations.

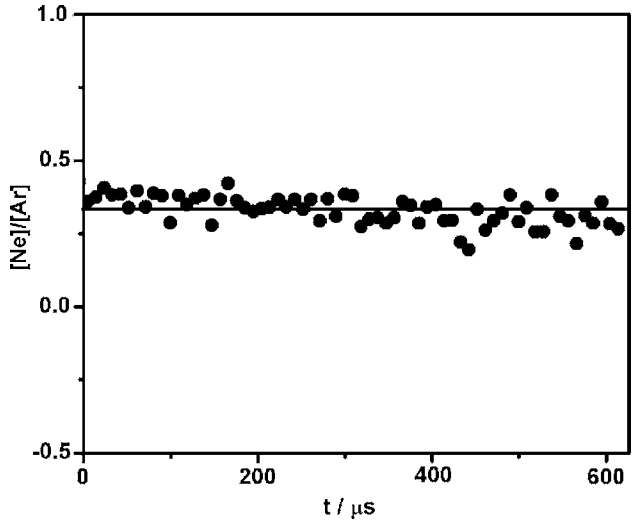

FIG. 8. Ne^+/Ar^+ peak area ratio vs time measured at $T_5=1788$ K with a 4% argon-neon mixture.

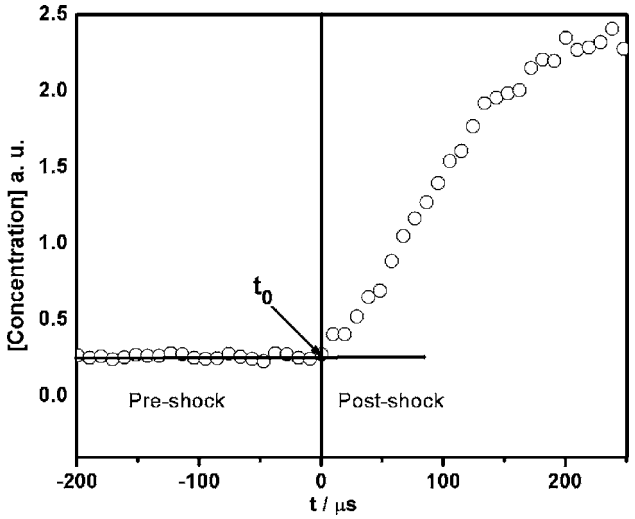

FIG. 9. The argon peak area (○) vs time for an experiment. The location of the time origin, t_0, corresponding to the formation of the reflected shock wave is indicated, using method 2 in the text.

Reaction (9) was investigated for $P_5 \approx 600$ and 1300 Torr, and $T_5=1260-1430$ K. Reaction mixtures were prepared containing 2% or 4% cyclohexene (99% Aldrich), and the same percentage of argon (99.999% AGA), as an internal standard, with the balance neon (99.999% AGA). The cyclohexene was degassed before use and the other species were used as supplied. To ensure homogeneity, the reaction mixture was allowed to stand for at least 24 h before use.

During an experiment data were acquired continuously for 1 ms and the ion source was pulsed at 50 or 105 kHz. The 50 kHz setting was used to obtain separated spectra without overlap between ionization events that were used to identify mass peaks. The 105 kHz setting generates an ion packet every 9.52 μs, improving the time resolution and is thus used to determine the rate of reaction. A sample data set is shown in Fig. 6 where the downward pointing spikes are the mass spectra and the upward spikes represent the timing signals captured on the DP306 digitizer. The first portion of the data set, to about 300 μs, is taken before the reflected shock wave is generated, the remainder from behind the reflected shock wave. The increase in signal that begins around 300 μs is then from the pressure buildup in the ion source caused by greater mass flow through the nozzle/skimmer interface from the high pressure behind the reflected shock wave. This inevitable rise in signal[8–15] is best accounted for by the use of an internal standard. Here argon has been used as the internal standard and all species of interest are scaled to its peak area, as suggested by Kern *et al.* and Krizancic *et al.*.[13,14] As neon and argon are inert and both are observed in the mass spectrum the ratio Ne^+/Ar^+ should be constant for a particular experiment and this is confirmed in Fig. 8.

Figure 5 shows a 20 μs time segment taken from the postshock region of Fig. 6, where the peaks corresponding to the major ions are identified. Note the excellent base line separation between ions that differ by $m/z=1$. The m/z for each peak is determined from

$$m/z = a(t_f)^2 + b, \tag{11}$$

where t_f is the time-of-flight for an ion relative to the ion extraction pulse, e.g., the falling edge of the timing pulse A in Fig. 5, and a and b are constants determined from measured t_f for known m/z, e.g., Ne^+ and Ar^+.

The raw data, as in Fig. 6, are processed to generate plots of relative peak area versus time for each species of interest where the peak areas are scaled by the internal standard as described above. The point in the profiles that corresponds to the formation of the reflected shock wave, t_0, is located by one of the two methods: In the first method t_0 is defined by Eq. (12).

$$t_0 = t_1 + t_2, \tag{12}$$

where t_1 is the time for the shock wave to travel from PT1, Fig. 1, to the orifice in the nozzle plate and t_2 is the time taken for a gas element to flow from the orifice to the center of the ion source. Here t_1 is either measured directly with a pressure transducer located in the nozzle plate or calculated by extrapolation of the shock velocity to the orifice. t_2 is estimated by combining the known distance between the end wall of the shock tube and the center of the ion source with the centerline velocity, V, taken from Eq. (4).

The second method of locating t_0 is simpler, providing that sufficient temporal resolution is available in the concentration/time profiles and that they are relatively smooth. Here t_0 is located at the point where the peak areas for nonreactive species, e.g., argon and neon, first show a sharp increase due to the pressure change in the ion source that occurs on formation of the reflected shock wave. An example of this latter method is shown in Fig. 9. Typically t_0 falls between two recorded points so the higher the time resolution in the species profiles, the more accurate its location. Generally, the simplicity of the second method is preferred when locating t_0, although both methods agree to within a few microseconds, less than the time resolution of the experiment.

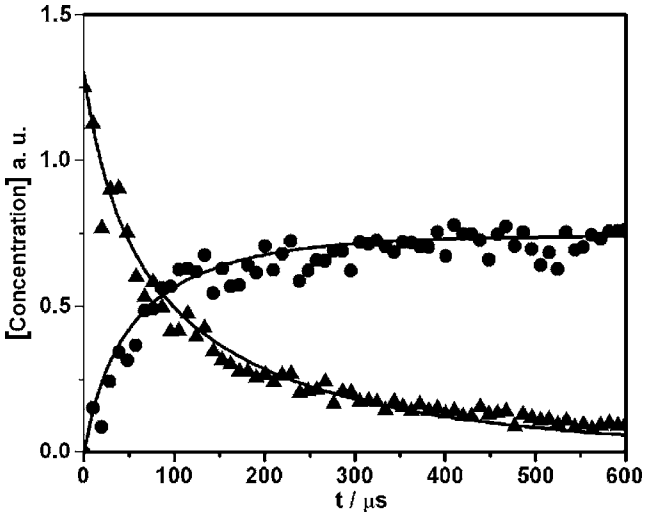

FIG. 10. Concentration time profiles for the reaction $C_6H_{10}=C_4H_6+C_2H_4$ at $P_5=619$ Torr, $T_5=1424$ K; (▲) cyclohexene; (●) ethylene; (—) simulation. Each point in the curve corresponds to one ionization cycle.

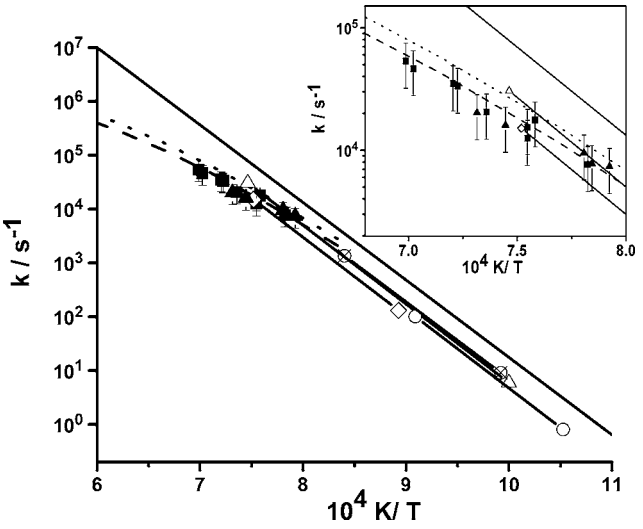

FIG. 11. Arrhenius plot and comparison of TOF-MS data with the literature: (■) this work at $P_5\approx600$ Torr; (▲) this work at $P_5\approx1300$ Torr; (○—○) Tsang (Ref. 41) at $P_5\approx1500-4500$ Torr; (△—△) Skinner *et al.* (Ref. 38) at $P_5\approx2200$ Torr; (◇—◇) Hidaka *et al.* (Ref. 40) at $P_5\approx1000-2300$ Torr (see text for comment on P_5); (⊗—⊗) from Barnard and Parrot (Ref. 39) at $P_5\approx1300$—2200 Torr; (– – –) and (···) from Ref. 37 for pressures of 107—170 and 360–550 Torr, respectively; (—) theoretical k_∞ from Ref. 37.

Once t_0 has been located, chemical kinetic simulations are used to determine the initial rate coefficients. Simulation is needed to account for nonisothermal effects arising from the enthalpy of reaction (9). The simulations were performed using the reflected shock model from a program designed to solve chemical kinetics behind incident and reflected shock waves. For the conditions in this work secondary reactions are suppressed and a single reaction was sufficient to model the system. An initial estimate of the rate coefficient was taken from Kiefer and Shah.[37] The rate coefficient was then varied iteratively to obtain the best fit between the simulation results and the experimental data for each experiment. A sample of the simulation results is shown in Fig. 10. The $[C_2H_4]$ profile is shown in addition to the $[C_6H_{10}]$ profile in Fig. 10 and the simulation predicts the profile well. This may seem a little surprising given the above comments on the fragmentation of species in the ion source; however, as the reaction proceeds, the contribution of C_6H_{10} fragments to the C_2H_4 peaks decreases and the contribution from C_4H_6 fragments to the C_2H_4 peaks increases counterbalancing the C_6H_{10} loss. Thus the C_2H_4 peaks increase against an almost constant background of fragments from other species.

The extracted rate coefficients for all the experiments are compared to literature data in Fig. 11. The agreement with these data is very good, in particular, with the results from Skinner *et al.*,[38] for 2200 Torr. The lower temperature data of Barnard and Parrot,[39] 1300–2200 Torr, have been extrapolated to our conditions and also show good agreement. The results from Hidaka *et al.*,[40] 1000–2300 Torr (incorrectly reported in the NIST database[42] as 100 Torr), are lower than the other data sets as was commented on by Kiefer and Shah.[37] As can be seen in Fig. 11, the results of the current experiments are about 30% lower than the 600 Torr LS results and there is virtually no rate variation between the 600 and 1300 Torr TOF-MS results. The small difference between the LS data and the TOF-MS results is not of great concern given the 20% scatter in the LS data points at the lower end of the temperature range[37] and the error bars of 30% in the present work. These error bars arise primarily from the location of t_0 and the scatter within the concentration/time profiles. Furthermore, experience has shown that LS experiments frequently overpredict rate coefficients at the lowest temperatures where the rate of reaction is small.

Rice-Ramsperger-Kassel-Marcus (RRKM) calculations using the model of Kiefer and Shah[37] were performed to examine the pressure dependency in the TOF-MS experiments and the effect of changing the bath gas from krypton in the LS experiments, to neon in the TOF-MS experiments. Over the temperature range of the results reported here the RRKM calculations predict differences of only a few percent in the rate coefficients as the pressure is increased from 600 to 1300 Torr, which would not be discernable in the TOF-MS experiments. The bath gas also has a negligible effect on the calculated rate coefficients.

The good agreement of the results from the ST/TOF-MS experiments with the literature data for cyclohexene decomposition demonstrates the ability to measure rate coefficients accurately at high temperatures and over a wide pressure range using the new ST/TOF-MS. The sampling of gases from the cold TBL which would lower the measured rate coefficients has been minimized with the differentially pumped nozzle/skimmer sampling system in good agreement with the theoretical analysis of the MBS. Thus the new ST/TOF-MS can be considered to be fully operational and suited for kinetic studies.

Future improvements to the apparatus will include the installation of different detector plates to improve the dynamic range of the MCP, thereby increasing the sensitivity of the instrument and increasing the pumping capacity in the expansion tank and ion source chamber to permit the use of larger nozzle and skimmer orifices to improve both the low

pressure, $P_5 < 300$ Torr, performance and to facilitate possible operation of the device in the incident shock.

ACKNOWLEDGMENTS

This work was performed under the auspices of the Office of Basic Energy Sciences, Division of Chemical Sciences, Geosciences, and Biosciences, U.S. Department of Energy, under Contract No. DE-AC02-06CH11357. Two of the authors (R.S.T. and J.H.K.) would also like to acknowledge support from the same agency under Contract Nos. DE-FE-85ER13384 and DE-FG02-85ER13384.

[1] *Handbook of Shock Waves*, edited by G. Ben-Dor, O. Igra, and A. Lifshitz (Academic, New York, 2001).
[2] J. Warnatz, in *Combustion Chemistry*, edited by W. C. Gardiner (Springer, New York, 1984).
[3] *Shock Waves in Chemistry*, edited by A. Lifshitz (Dekker, New York, 1981).
[4] G. Gaydon and I. R. Hurle, *The Shock Tube in High-Temperature Chemical Physics* (Reinhold, New York, 1963).
[5] J. N. Bradley, *Shock Waves in Chemistry and Physics* (Wiley, New York, 1962).
[6] D. L. Baulch *et al.*, J. Phys. Chem. Ref. Data **21**, 416 (1992).
[7] W. Tsang and R. F. Hampson, J. Phys. Chem. Ref. Data **15**, 1087 (1986).
[8] J. N. Bradley and G. B. Kistiakowsky, J. Chem. Phys. **35**, 256 (1961).
[9] J. E. Dove and D. McL. Moulton, Proc. R. Soc. London, Ser. A **283**, 216 (1965); D. McL. Moulton, Ph.D. thesis, Harvard University, 1964.
[10] P. Modica, J. Chem. Phys. **69**, 2111 (1965).
[11] R. W. Diesen and W. J. Felmlee, J. Chem. Phys. **39**, 2115 (1963).
[12] S. C. Barton, M. A. DiValentin, and J. E. Dove, Proceedings of the Fifth International Shock Tube Symposium, 1965, p. 739.
[13] R. D. Kern, H. J. Singh, and Q. Jhang, in *Handbook of Shock Waves*, edited by G. Ben-Dor, O. Igra, and A. Lifshitz (Academic, New York, 2001), Vol. 3, Chap. 16.1; R. D. Kern, Ph.D. thesis, University of Texas, 1965.
[14] Krizancic, M. Haluk, S. H. Cho, and O. Trass, Rev. Sci. Instrum. **50**, 909 (1979).
[15] P. R. Ryason, Rev. Sci. Instrum. **28**, 607 (1967).
[16] P. Rouveirolles, R. Lisbet, and R. Foulatier, J. Phys. E **17**, 586 (1984).
[17] R. D. Kern, H. Chen, J. H. Kiefer, and P. S. Mudipalli, Combust. Flame **100**, 177 (1995).
[18] J. A. Miller and S. J. Klippenstein, J. Phys. Chem. A **107**, 7783 (2003).
[19] S. E. Stein, J. A. Walker, M. Suryan, and A. Fahr, Twenty-third Symposium (International) on Combustion, The Combustion Institute (1990), p. 85.
[20] U. Alkemade and K. H. Homann, Z. Phys. Chem. (Munich) **19**, 161 (1989).
[21] W. Tang, R. S. Tranter, and K. Brezinsky, J. Phys. Chem. A **109**, 6056 (2005).
[22] B. R. Giri, H. Hippler, M. Olzmann, and A. N. Unterreiner, Phys. Chem. Chem. Phys. **5**, 4641 (2003).
[23] S. M. Hurst and S. H. Bauer, Rev. Sci. Instrum. **64**, 1342 (1993).
[24] L. Davies, British Aeronautical Research Council Report No. CP880, 1967, Pt. I.
[25] R. J. Cotter, in *Time-of-Flight Mass Spectrometry*, ACS Symposium Series Vol. 549, edited by R. J. Cotter (ACS, Washington, DC, 1994).
[26] G. J. Williams and R. G. Wilkins, Combust. Flame **21**, 325 (1973).
[27] D. J. Hucknall and A. Morris, *Vacuum Technology Calculation in Chemistry* (Royal Society of Chemistry, Cambridge, UK, 2003).
[28] H. Ashkenas and F. S. Sherman, in *Fourth International Symposium on Rarefied Gas Dynamics*, edited by J. H. deLeeuw (Academic, New York, 1966), p. 84.
[29] B. Anderson, in *Molecular Beams and Low Density Gas Dynamics*, edited by P. P. Wegener (Dekker, New York, 1974), pp 1–91.
[30] C. A. Stearns, F. J. Kohl, G. C. Fryburg, and R. A. Miller, in Tenth Materials Research Symposium on Charcterization of High Temperature Vapours and Gases, 1979, NBS Special Publication 561/1, p. 303.
[31] G. Scoles, *Atomic and Molecular Beam Methods* (Oxford University Press, New York, 1988), Vol. 1.
[32] G. E. McMichael and J. B. French, Phys. Fluids **9**, 1419 (1966).
[33] B. French and G. E. McMichael, in *Fifth International Symposium of Rarefied Gas Dynamics*, edited by E. L. Brundin (Academic, New York, 1969), p. 1385.
[34] E. C. Voldner and O. Trass, J. Chem. Phys. **73**, 1601 (1980).
[35] E. C. Voldner and O. Trass, in Proceeding of 11th International Symposium on Shock Tubes and Waves, 1977, p. 490.
[36] H. W. Liepmann, J. Fluid Mech. **10**, 65 (1961).
[37] J. H. Kiefer and J. N. Shah, J. Phys. Chem. **91**, 3024 (1987).
[38] G. B. Skinner, D. Rogers, and K. B. Patel, Int. J. Chem. Kinet. **13**, 481 (1981).
[39] J. A. Barnard and T. K. Parrot, J. Chem. Soc., Faraday Trans. **72**, 2404 (1976).
[40] Y. Hidaka, T. Chimori, S. Shiba, and M. Suga, Chem. Phys. Lett. **111**, 181 (1984).
[41] W. Tsang, Int. J. Chem. Kinet. **2**, 311 (1970).
[42] S. E. Stein, NIST Mass Spec Data Center, in *NIST Chemistry WebBook*, NIST Standard Reference Database Number 69, edited by P. J. Linstrom and W. G. Mallard (National Institute of Standards and Technology, Gaithersburg, MD, 2005) (http://webbook.nist.gov).